Self-healing thermal barrier coating systems fabricated by spark plasma sintering

Nozahic, Franck; Estournès, Claude; Carabat, Alexandra Lucia; Sloof, Willem G.; van der Zwaag, Sybrand; Monceau, Daniel

DOI
10.1016/j.matdes.2018.02.001

Publication date
2018

Document Version
Final published version

Published in
Materials & Design

Citation (APA)
Nozahic, F., Estournès, C., Carabat, A. L., Sloof, W. G., van der Zwaag, S., & Monceau, D. (2018). Self-healing thermal barrier coating systems fabricated by spark plasma sintering. *Materials & Design*, *143*, 204-213. https://doi.org/10.1016/j.matdes.2018.02.001

Materials and Design 143 (2018) 204–213

Contents lists available at ScienceDirect

Materials and Design

journal homepage: www.elsevier.com/locate/matdes

Self-healing thermal barrier coating systems fabricated by spark plasma sintering

Franck Nozahic [a,b], Claude Estournès [b,*], Alexandra Lucia Carabat [c], Willem G. Sloof [c], Sybrand van der Zwaag [d], Daniel Monceau [a]

[a] CIRIMAT, Université de Toulouse, CNRS, INPT, UPS, ENSIACET, 4 allée Emile Monso, BP-44362, 31030 Toulouse Cedex 4, France
[b] CIRIMAT, Université de Toulouse, CNRS, INPT, UPS, 118 Route de Narbonne, F-31062 Toulouse, France
[c] Department of Materials Science and Engineering, Delft University of Technology, Mekelweg 2, 2628 CD Delft, The Netherlands
[d] Faculty of Aerospace Engineering, Delft University of Technology, Kluyverweg 1, 2629 HS Delft, The Netherlands

HIGHLIGHTS

- TBC made of YPSZ and encapsulated $MoSi_2$(Al,B) particles was spark plasma sintered on MCrAlY coated Ni-based superalloys.
- TBC self-healing ability was proved with cracks locally filled with silica and a zircon phase that links the crack surfaces
- Al_2O_3 shell protects the $MoSi_2$-based particles against premature oxidation under thermal cycling conditions at 1100 °C in air.
- Detrimental reaction between $MoSi_2$ particles and MCrAlY bond coating may occur but preventive solutions have been found.
- After high temperature exposure the initial protective Al_2O_3-shell around the particles is converted to more complex shell.

GRAPHICAL ABSTRACT

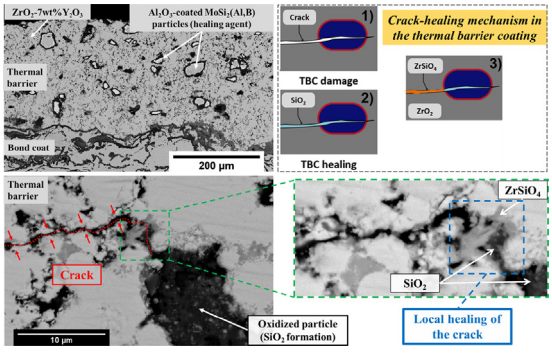

ARTICLE INFO

Article history:
Received 7 November 2017
Received in revised form 31 January 2018
Accepted 1 February 2018
Available online 2 February 2018

Keywords:
Spark plasma sintering
Self-healing thermal barrier coatings
High-temperature cyclic oxidation
Intermetallic particles
Multi-layer materials
Ceramic matrix composites

ABSTRACT

The present paper focuses on the Spark Plasma Sintering (SPS) manufacturing of a new type of self-healing thermal barrier coating (TBC) and a study of its thermal cycling behaviour. The ceramic coating consists on an Yttria Partially Stabilized Zirconia (YPSZ) matrix into which healing agents made of $MoSi_2$-Al_2O_3 core-shell particles are dispersed prior to sintering. The protocol used to sinter self-healing TBCs on MCrAlY (M: Ni or NiCo) pre-coated Ni-based superalloys is described and the reaction between the particles and the MCrAlY bond coating as well as the preventive solutions are determined. Thermal cycling experiments are performed on this complete multi-layer system to study the crack healing behaviour. Post-mortem observations highlighted local healing of cracks due to the formation of silica and the subsequent conversion to zircon at the rims of the cracks.

* Corresponding author at: Equipe NNC, CIRIMAT-UPS-CHIMIE, Université Toulouse 3 - Paul Sabatier, 118 Route de Narbonne, F-31062 Toulouse, France.
E-mail address: estourne@chimie.ups-tlse.fr (C. Estournès).

https://doi.org/10.1016/j.matdes.2018.02.001
0264-1275/

1. Introduction

Thermal Barrier Coatings (TBCs) made of Yttria Partially Stabilized Zirconia (YPSZ), deposited by Electron Beam Physical Vapour Deposition (EBPVD) or plasma-spraying techniques onto metallic superalloy turbine blades, are widely used to increase the durability of internally cooled hot-section metal components in advanced gas-turbines for aircrafts and power generation [1–4]. The role of such a ceramic coating is to act as a thermal insulator by decreasing the temperature of the underlying Ni-based superalloy blade material. The TBC is deposited on a bond coating that promotes and maintains the adhesion of the TBC and provides oxidation resistance to the system due to the formation of a Thermally Grown Oxide (TGO) consisting mainly of α-Al_2O_3. The failure of plasma sprayed TBCs under thermal cycling is a complex phenomenon that is mainly due to the stresses induced by the mismatch between thermal expansion coefficients of the different components of the TBC system and/or by the growth of the α-Al_2O_3 TGO as a result of the oxidation of the underlying bond coating. In case of plasma sprayed TBCs deposited on bond coatings with high surface roughness, failure was shown to be controlled by a sequence of initiation, propagation and coalescence of cracks, just above the TGO, that finally leads to the spallation of the TBC and expose the hot-section metal components to the high-temperature environment [5]. Hence, a TBC with higher toughness value or that exhibits self-repair ability at high temperature in an oxidizing environment is highly desirable to extend its lifetime and enhance its reliability.

Recently, embedment of SiC particles was shown to be a promising way to increase the toughness of brittle materials such as silicon nitride (Si_3N_4), alumina (Al_2O_3) or mullite ($3Al_2O_3 \cdot 2SiO_2$) but also to provide a self-healing ability to these materials [6–8]. When cracks interact with SiC particles, these latter react at high temperature with oxygen leading to the formation of an expanding silica based reaction product that will flow into the crack. Another example is given by the self-healing of nano Ni particles reinforced alumina composites [9]. To create an autonomously self-healing TBC, the material chosen as healing agent must satisfy some criteria: (i) it should have a high melting point, higher than the maximum operating temperature for TBCs (1000 °C or above) and a thermal expansion coefficient that matches reasonably with the one of the TBC material, (ii) it should be able to oxidize and form a liquid which fills the crack and establishes direct contact with the TBC crack surfaces, (iii) the wetting of the crack surfaces should be followed by a solid state chemical reaction between the liquid and the TBC material leading to the formation of a load bearing material [10]. Based on a literature study of potential healing agents, boron doped $MoSi_2$ particles covered with an alumina shell have been proposed as healing agents for TBC [10,11]. When intercepted by cracks, the healing agent will oxidize leading to the formation of a low viscosity and amorphous borosilicate phase that will flow into the cracks. Subsequently, this phase will react with the surrounding ZrO_2-based TBC to form a load bearing and crystalline $ZrSiO_4$ phase that closes the crack gap and exhibits a strong adhesion with the fracture surfaces. However, industrial ZrO_2-based TBCs are porous (≈20 vol%) and known as being an excellent oxygen ion conductor at elevated temperatures [12,13], thus encapsulation of the $MoSi_2$ particles by a high temperature stable and oxygen impenetrable shell is highly desirable to prevent the spontaneous oxidation of these particles. It has been proposed to deposit a shell of alumina around the $MoSi_2$ based particles via a precipitation process [14] or via a sol-gel process [15].

Recently, it was demonstrated the feasibility to deposit mixed layers of $MoSi_2$ based particles and YPSZ by Atmospheric Plasma Spraying (APS) technique leading for the optimal process conditions to a significant life time extension [16]. While APS is a suitable technique for coating complex shaped components, the Spark Plasma Sintering (SPS), has attracted great interest for the manufacturing of multi-layer samples for scientific studies on material degradation under relevant thermal cycles [17]. Already the feasibility of one-step manufacturing of YPSZ nanocrystalline TBC and Pt-rich γ-Ni/γ'-Ni_3Al bond coating sintered on AM1 substrates was demonstrated [18]. Thereafter, the same protocol was used to fabricate complete TBC systems with a NiCrAlY bond coating [19]. SPS was also used to simultaneously produce YPSZ/MCrAlY multi-layer coatings on Hastelloy X substrates with a rough YPSZ/MCrAlY interface [20]. Recently, the feasibility of functionally graded TBC by SPS was reported [21].

The aim of the present study is to evaluate the self-healing of model TBC systems. For this purpose, SPS technique was first used to sinter mixtures of YPSZ powder and $MoSi_2$ co-doped with B and Al based particles on a NiCoCrAlY coated Ni-based superalloy. Prior to sintering, these particles were coated with an α-Al_2O_3 protective shell deposited via a sol-gel route. The particles were alloyed with Al to allow the formation of Al_2O_3, by selective oxidation of Al, in case of shell breakage during the SPS sintering. The nature and composition of the protective shell, before and after SPS sintering and short annealing treatment, were characterized by means of X-ray Diffractometry (XRD), Scanning Electron Microscopy (SEM) and Transmission Electron Microscopy (TEM). Thermal cycling tests were performed in order to study the behaviour and the self-healing response of the model self-healing TBC systems. The advantage of the SPS method over the industrially more relevant APS method is that the protective alumina coating on the $MoSi_2$ healing particles remains intact during the synthesis process. The integrity of the particle coating is crucial to ensure the absence of non-crack related decomposition of the particle [22,23].

To the best of authors' knowledge, this paper presents for the first time a complete study showing: i) the manufacturing and investigation of the thermal cycling behaviour and ii) the crack healing of self-healing TBC made by SPS.

2. Experimental procedure

2.1. Synthesis of the encapsulated $MoSi_2$(B) based healing particles

Coating of the $MoSi_2$ based intermetallic particles was performed using a modified Yoldas method [15], based on the polycondensation and formation of boehmite sol. The $MoSi_2$ based particles (with 99.5% purity) were alloyed with 2 wt% B and 6 wt% Al and delivered by ChemPur GmbH, Karlsruhe, Germany. The starting materials used for this sol-gel synthesis were: aluminium tri-sec-butoxide ($Al(OCH(CH_3)C_2H_5)_3$, 97% purity, Sigma Aldrich Co. LLC, St. Louis, MO) as a precursor, nitric acid (HNO_3 solution, Sigma-Aldrich Co. LLC, St. Louis, MO), isopropanol (99.8%, Sigma-Aldrich Co., LLC, St. Louis, MO), ethanol (99.8%, Sigma-Aldrich Co., LLC, St. Louis, MO), and deionized water (18.2 MΩ·cm at 25 °C). All these chemicals were used without any further purification.

Prior to the encapsulation process, the $MoSi_2$ based powder was wind sifted to remove the fine fraction. Wind sifting was performed using an Alpine 100 MRZ laboratory zig-zag classifier (Alpine Multi-Plex 100 MRZ, Hosokawa Micron Powder System, Summit, New Jersey, USA). Airflow was fixed at 15 m^3/h and the classifier rotational speed was kept at 5000 rpm. The particle size distribution was measured with laser diffraction using a Malvern Mastersizer X (Malvern Instruments Ltd., Worcestershire, UK). Prior to this measurement, the particles were dispersed in deionized water for 20 min by applying ultrasonic vibration. The wind sifting resulted in a powder having an average particle diameter of 33 μm and 16 and 60 μm at 10 and 90% cut-off, respectively.

The coating process of the $MoSi_2$ based powder was done by first heating a mixture of 600 mL of deionized water and 15 mL of 1.0 M HNO_3 to 80 °C to obtain a molar ratio of 2:150 of $Al(OC_4H_9)_3$ to H_2O. First, 10 g of $MoSi_2$ powder was added to the solution mixture of deionized water and HNO_3 and 200 sccm nitrogen (5 N purity) was purged through the suspension to improve the dispensability of the particles in the solution. When the temperature was stable at 80 °C again, 10 g of $Al(OC_4H_9)_3$ was added with approximately 25 mL of ethanol to

transfer the viscous liquid into the beaker. After, the system was left to gelate for 60 min. Next, the nitrogen flow and stirring were stopped and the solution was left at 80 °C until the liquid fraction was evaporated. The resulting gel was filtered using a glass-vacuum filtration system (Sartorius Stedium, Biotech, Goettingen, Germany) with a hydrophilic propylene membrane with a pore size of 0.45 μm. To remove the unreacted precursors, the coated powder was washed with warm deionized water (about 60 °C). Next, the coated particles were dried in an autoclave (WTC binder, Tamson, Tuttlingen, Germany) at 110 °C overnight and gently ground to break up the agglomerates. Thereafter, the sol-gel coated particles were subjected to two-steps annealing treatment. First, a calcination treatment was applied at 450 °C for 15 h under argon, in order to slowly release the molecular water, followed by a post-treatment at 1200 °C for 1 h under argon to consolidate the shell and to promote the formation of α-Al_2O_3. The particles are alloyed with 6 wt% Al to allow the formation of alumina by selective oxidation at sites where the shell may be damaged during the annealing treatments and/or sintering.

2.2. Preparation of YPSZ composite with encapsulated $MoSi_2$(B) based healing particles

A composite made of a YPSZ matrix containing 10 vol% of encapsulated $MoSi_2$(B) based healing particles was prepared in order to characterize the microstructure and the composition of the shell deposited via sol-gel route. Prior to sintering, appropriate amounts of YPSZ powder (AMPERIT 827.774, ZrO_2_7 wt%Y_2O_3) and encapsulated $MoSi_2$ (B) based particles were mechanically dry mixed for 1 h in a Turbula-type powder blender. Prior to mixing, the YPSZ powder was downsized from a D_{50} of 40 μm to 7 μm, by using a Retsch PM 100 planetary ball milling, to improve its sinterability. Then, the powder mixture was sintered in a 15 mm in diameter graphite die for 20 min at a temperature of 1150 °C and under a constant and uniaxial compaction pressure of 110 MPa applied since the beginning of the sintering cycle. A Dr. Sinter SPS-2080 equipment (SPS Syntex Inc., Kanagawa, JP) located at the Plateforme Nationale de Frittage Flash CNRS (PNF^2, Université Toulouse III Paul Sabatier, France) was used to densify the material. The as-prepared composite was then annealed for 24 h at 1100 °C under argon in order to promote the selective oxidation of Al from the $MoSi_2$ (B) based particles. The low oxygen partial pressure is expected to foster the growth of α-Al_2O_3 instead of any other transition phase of alumina [24] and help repairing of micro-cracks in the protective shell that may have been initiated during SPS process.

2.3. Preparation of self-healing TBCs with encapsulated $MoSi_2$(B) based healing particles

The substrates used in this study were 24.5 or 20 mm in diameter discs made of Ni-based superalloys (Hastelloy X). Bond coatings of 200 μm in thickness were deposited using APS or HVOF techniques with optimized parameters. For the APS bond coating, the NiCrAlY powder used (Amdry 962) contains 22 wt% Cr, 10 wt% Al, and <1.2 wt% Y. The NiCoCrAlY powder used for deposition of the bond coating by HVOF is a commercially available powder (Amperit 410) that contains 23 wt% Co, 17 wt% Cr, 13 wt% Al, and <0.7 wt% Y. The roughness (R_a) of the NiCrAlY and NiCoCrAlY bond coatings were derived from metallographic images of cross-sections of the MCrAlY coated substrates in the as-sprayed conditions [25]. High level of roughness (5 μm and 9 μm, respectively) have been obtained which is common for industrial applications. A commercially available YPSZ powder (Amperit 827.774) was used for the fabrication of the TBC systems. The average YPSZ particle size was reduced to increase its sinterability from 40 to 7 μm with a Retsch PM 100 planetary ball mill using zirconia balls and jar.

Prior to sintering of the TBC, YPSZ powder and 10 vol% of encapsulated $MoSi_2$(B) based particles were mixed following the protocol described above. Then, graphite dies of 24.5 or 20 mm inner diameter covered with a graphite foil (Papyex® Mersen) were filled according to the assembly drawing depicted in Fig. 1. Previous studies [26,27] reported the existence of a thermal gradient between the surface of the graphite die and the sample. For this reason, two alumina layers were placed on either side of the assembly, thus the electric current goes mainly through the graphite die during SPS process. This way, a more homogeneous heating of the assembly is expected [18,28]. The sintering of the assembly was completed with a fixed heating rate of 100 °C·min^{-1}, up to 1150 °C, with a soaking time of 20 min at this temperature and under a constant macroscopic and uni-axial compaction pressure of 110 MPa applied since the beginning of the sintering cycle. The temperature was monitored by an optical pyrometer focused on a small hole (3 mm in depth) located at the external surface of the die. The electric current was applied by pulses following the standard 12/2 (on/off 3.3 ms) pulse pattern. The TBC systems were then annealed for 24 h at 1100 °C under argon to promote the selective oxidation of Al from the $MoSi_2$ based particles. A desired level of about 20 vol% porosity in the TBC after SPS is obtained, which is close to the porosity of industrial APS TBCs.

Thermal cycling of each TBC system was performed in laboratory air. A thermal cycle is composed of a fast heating up to 1100 °C (<10 min.) by moving samples into the hot furnace for a duration of 1 or 24 h. Then the samples were removed from the furnace and forced air cooling (15 min.) was applied. The specimens were inspected daily and samples showing massive delamination were removed prior to exposure to a next thermal cycle. The failed TBC systems were mounted in epoxy resin, cut and polished with 1 μm diamond suspension prior to metallographic observations.

3. Characterization

The shell and core compositions of the healing particles were analysed with X-ray diffractometry. A Bruker D500 diffractometer equipped with a Huber incident beam monochromator and a Braun PSD detector operated with Cu Kα1 (154.060 pm wavelength) was used to record the diffractograms in the 2θ range of 15 to 80° with a step size of 0.0387°2θ.

A transmission electron microscope (JEOL JSM 2100) coupled with an Energy Dispersive Spectrometer (EDS, Aztec Advanced equipped) for X-ray Micro Analysis (XMA) was employed to analyse the microstructure and the composition of the protective shell after SPS and annealing of the self-healing TBC. Prior to the TEM investigation, a thin lamella across the YPSZ/particle interface was prepared using a SEM (FEI HELIOS 600i) equipped with a Focused Ion Beam (FIB).

The cross-sections of the TBC systems were examined with SEM (LEO435VP) equipped with an EDS (Imix-PC, PGT) for XMA. Image analysis was performed using the "Image J" software to measure the particle diameters. When a specimen is cut, the cross-section does not necessarily pass through the middle of the particles. For this reason, a correction factor (≈1.21) corresponding to the relative error between the measured diameter and the real diameter of the particles was applied [29].

4. Results and discussion

4.1. Shell composition of encapsulated $MoSi_2$ based particles

To preserve the integrity of the shell during annealing, the encapsulated particles were first exposed at 450 °C, to gradually release the molecular water from the gel, and to prevent shell cracking during annealing at 1200 °C for 1 h in Ar, to convert the shell into α-Al_2O_3. According to the XRD results, the core of the $MoSi_2$ based particles remained intact; see Fig. 2. After exposure at 1200 °C, α-Al_2O_3 and some $Al_{18}B_4O_{33}$ of the shell were observed and tetragonal $MoSi_2$ as the main constituent of the core of the particle. Minor amounts of Mo_5Si_3 and Mo_xB_y in the core of the particles were identified. Also, some remnant hexagonal $Mo(Si,Al)_2$ was detected.

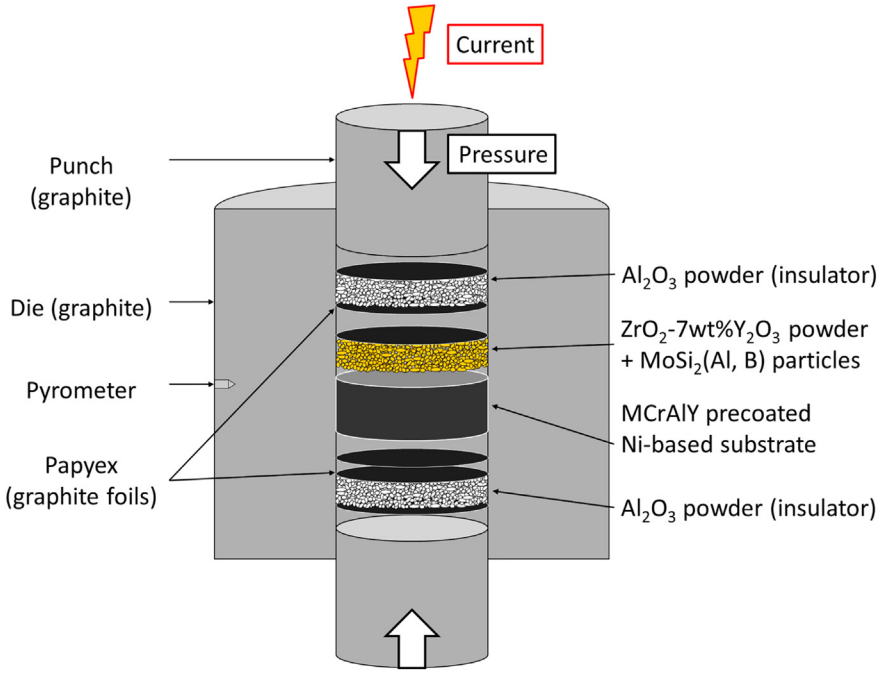

Fig. 1. Schematic arrangement of materials in the graphite die for manufacturing of self-healing TBCs with spark plasma sintering (SPS).

The shell microstructure of encapsulated $MoSi_2$(B) based particles in the YPSZ composite prepared by SPS and after annealing in Ar at 1100 °C for 24 h is shown in Fig. 3. The YPSZ matrix consists of tetragonal zirconia as determined by XRD. A desired level of about 20 vol% porosity in the YPSZ matrix after SPS is obtained, which is close to the porosity of industrial APS TBCs. A cross-section view of the embedded encapsulated $MoSi_2$ based particles is seen in Fig. 3(a). Although there is a (small) mismatch in the values of the published coefficients of thermal expansion (CTE) of YPSZ (10.5×10^{-6} °C^{-1} [30]) and $MoSi_2$ (8.1×10^{-6} °C^{-1} [31]), no visible cracks were observed in the densified composite. This is consistent with our previous work on YPSZ composites containing $MoSi_2$ inclusions prepared by SPS [22]. A continuous dark phase with an average thickness of 0.7 μm was observed around the $MoSi_2$ based particles. This phase corresponds to the protective shell that was deposited via the sol-gel route onto the particles and also formed during annealing by selective oxidation of Al contained in the $MoSi_2$. TEM observations of a representative area of the interface between YPSZ and the particle are shown in Fig. 3(b) and (c). The core of the $MoSi_2$ particles is composed of two phases, viz. t-$MoSi_2$ and t-Mo_5Si_3. The latter is present inside the particle but also forms a continuous layer around the particle with a thickness of about 100 nm. This layer is expected to form during deposition of the protective shell or during SPS process followed by annealing treatment as results of the selective oxidation of the silicon from the $MoSi_2$ based particle according to the following equation [32]:

$$5\ MoSi_{2(s)} + 7\ O_{2(g)} \rightarrow Mo_5Si_{3(s)} + 7\ SiO_{2(s)} \quad (1)$$

The second oxidation product, which is silica, can be observed as a continuous layer with an average thickness of 300 nm on top of the Mo_5Si_3 phase. The silica scale is amorphous and enriched with nanoparticles identified as MoO_2 of about 5 nm in diameter. This implies that despite the establishment of a continuous layer of silica and the low oxygen partial pressure at the Mo_5Si_3/SiO_2 interface, Mo can oxidize and escape as gaseous species. This observation is consistent with a previous study [33]. The EDS did not allow to detect the presence of B due to its low atomic number. However, many researchers reported the formation of a borosilicate phase when B enriched $MoSi_2$ materials are oxidized at high temperatures in air [34–38]. The presence of boron oxide within silica is responsible for the decrease of the melting temperature and the viscosity of this oxide [35]. This could also help the evacuation of Mo oxide volatile species. Al and Si rich oxides with Mo and Y were also detected meaning that the borosilicate phase reacted with the Y_2O_3 from YPSZ and Al_2O_3 or Al from the protective shell or the particle, respectively. The globular shape of these phases indicates that they are likely in liquid-state at the annealing temperature of 1100 °C.

An additional layer composed of γ-Al_2O_3 crystallites with an average diameter of 280 nm and $ZrSiO_4$ crystallites was observed; see Fig. 3(d). This structure for alumina is unexpected even after quite a long annealing at a temperature of 1100 °C. The presence of other elements might be responsible for preventing the transformation of γ into α-Al_2O_3. $ZrSiO_4$ crystallites formed as a result of the reaction between the silica like phase and the surrounding ZrO_2-based TBC and according to [39]:

$$SiO_{2(s)} + ZrO_{2(s)} \rightarrow ZrSiO_{4(s)} \quad (2)$$

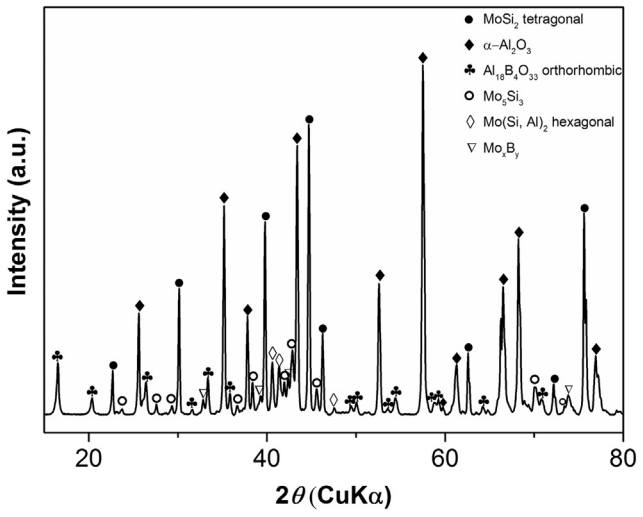

Fig. 2. Diffraction pattern of encapsulated $MoSi_2$ based particles alloyed with 2 wt% B and 6 wt% Al after annealing at 1200 °C for 1 h in Ar.

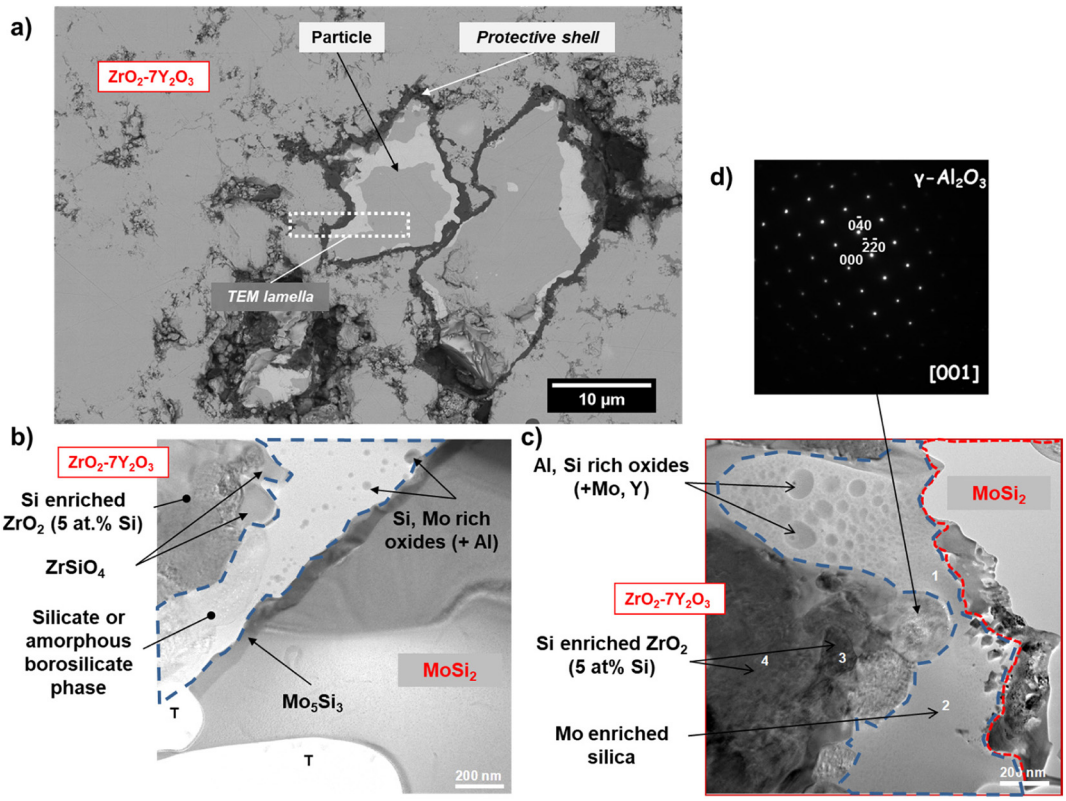

Fig. 3. Composite of encapsulated $MoSi_2$(B) based healing particles embedded in YPSZ after annealing in Ar at 1100 °C for 24 h: (a) cross-section of the composite just before lift-out of a thin FIB lamella. (b) and (c) TEM images of the FIB lamella after final thinning. (d) diffraction pattern of a γ-Al_2O_3 crystallite. Here, 'T' denotes some undesirable pores introduced during the thinning process.

The formation of $ZrSiO_4$ at temperatures as low as 1100 °C from annealing of cold pressed mixtures of $MoSi_2$ and YPSZ or YPSZ/$MoSi_2$ multi-layer samples has been reported previously [23,40]. A silicon enriched area was also identified close to the YPSZ matrix. This could be explained by the formation and the flowing of a low viscosity borosilicate phase, during the sintering or the annealing treatment, that wetted the zirconia grain boundaries.

The protective shell around the $MoSi_2$(B) based healing particle embedded in YPSZ by SPS is thus composed of a stack of several discrete oxide scales rather than a continuous and uniform layer of α-Al_2O_3. An oxygen-impenetrable barrier between $MoSi_2$(B) and YPSZ is mandatory to ensure long term stability of the particle and thus to prevent premature oxidation of $MoSi_2$(B), even in absence of cracks. A compilation of data from the literature related to the oxygen diffusion coefficient (D) values in different oxides is shown in Fig. 4. One can observe that the lowest value for D pertains to α-Al_2O_3 which motivated the choice to deposit such oxide as a continuous layer around the particles to protect them against oxidation [11]. TEM observations highlighted the presence of $ZrSiO_4$ and γ-Al_2O_3 crystallites; see Fig. 3(b) and (c). The D value for $ZrSiO_4$ is also low meaning that $ZrSiO_4$ could protect the particles against oxidation but with a more limited effect compared to α-Al_2O_3. However, being discontinuous, the oxide layer formed with these oxides is not expected to be an extremely efficient diffusion barrier against oxygen.

A continuous layer made of a borosilicate phase was observed around the particles; see Fig. 3(b). However, the D value for SiO_2-B_2O_3 is several decades higher than those for α-Al_2O_3 or $ZrSiO_4$, which suggests that it is not expected to be an effective protective shell for the particles. Therefore, it is of interest to perform long duration exposures of the particles at high temperature in order to assess the effectiveness of the different oxides as protective shell and consequently the stability of the particles.

4.2. Silicide formation, consequences and prevention

A first attempt to prepare self-healing TBCs was made by sintering a mixture of YPSZ and 20 vol% of $MoSi_2$ based particles as TBC on a NiCoCrAlY coated Hastelloy X substrate by using the sintering cycle previously described for the manufacturing of complete TBC systems. Fig. 5 shows a cross-section view of this system after manufacturing. One can observe a well densified reaction zone of about 45 µm in thickness between the TBC and the BC. According to XMA, the bright grey phase between the YPSZ grains corresponds to a solid solution of Ni, Co and Si. These silicides are expected to form during the SPS process as a result of the reaction between the $MoSi_2$ based particles and the NiCoCrAlY bond coating. The formation and growth of silicides with poor mechanical properties, that fill the pores of the TBC making it less strain compliant, leads to fast spalling of the TBC after SPS process or after few thermal cycles. Thus, the formation of silicides at the YPSZ/BC interface is detrimental for the lifetime of the TBC.

The growth of Ni silicides is known to be controlled by Ni diffusion [49–51]. Co is the major diffusing specie during the growth of $CoSi_2$ [52], while the growth of CoSi is controlled by Si diffusion [52]. These diffusion-controlled growth processes involving Ni or Co are in good agreement with our experimental observations of the initial bond coating - TBC interface; see Fig. 5. This formation of silicides was also observed with smaller amounts of $MoSi_2$ particles, down to 5 vol%, even if the contact between the bond coating and the particles is limited. It might be the case that during SPS and more especially during heating that the $MoSi_2$(B) based particles oxidize, leading to the formation of a low viscosity borosilicate phase that flows between the unconsolidated YPSZ grains and came into contact with the Ni and Co from the bond coating making a fast diffusion channel for these elements. Furthermore, there is a eutectic point at 964 °C for the Ni-Si system which is almost 200 °C below the sintering temperature [53]. All these aspects explain the relatively fast growth kinetics of the silicide scale.

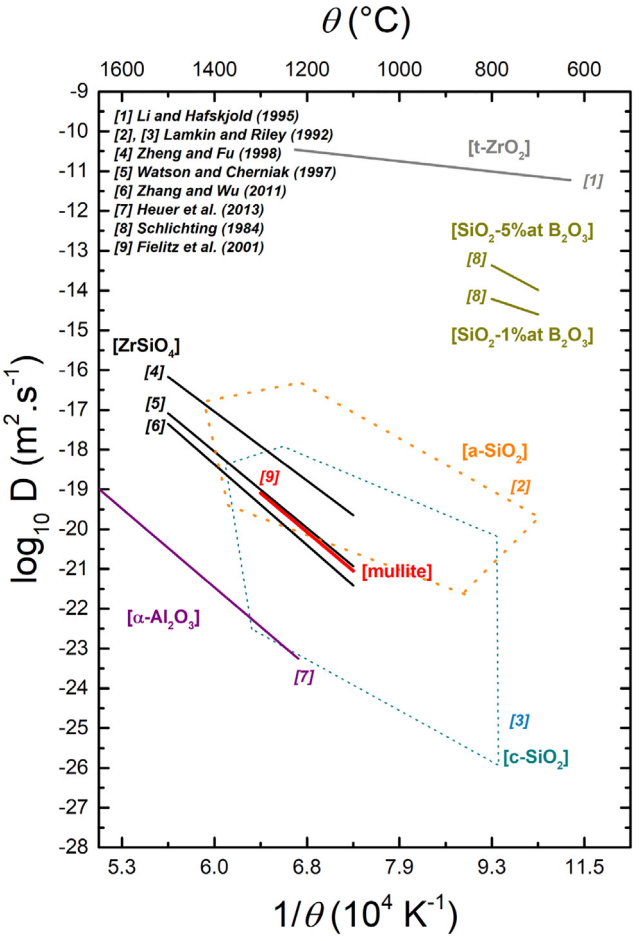

Fig. 4. Diffusion coefficient of oxygen D as a function of temperature θ for zirconia [41], silica [42], mullite [43], alumina [44] and zircon [45–47]. Domains for oxygen diffusion in amorphous and crystalline silica are reproduced from Ref. [48].

In order to prevent the formation of the silicide phases, the MCrAlY coated substrates were pre-oxidized at 1100 °C in "air" vacuum (i.e. 3.10^{-3} Pa). This thermal treatment promotes the formation of a thin α-Al_2O_3 oxide scale (0.9 μm) on top of the bond coating that will act as a physical-chemical barrier between the particles and the bond coating. An annealing treatment consisting of 2 h in 'air' vacuum at 1100 °C followed by 5 h in air at the same temperature was shown to be enough to prevent the formation of silicides. All MCrAlY coated substrates were consequently pre-oxidized according to the previously described annealing treatment prior to the sintering of the TBC top coat.

4.3. Thermal cycling behaviour and crack healing

A series of top views of a TBC made of a mixture of 10 vol% of encapsulated $MoSi_2$(B) based particles and YPSZ is shown in Fig. 6 and highlights the evolution of the damage during thermal cycling of the TBC coated system. One can observe that there is no spallation of the TBC even after 1084 cumulated hours (30 cycles) at 1100 °C. Failure of the system is observed after 31 cycles at 1100 °C which is associated with the spalling of almost half of the TBC. Fig. 7(a) shows that the TBC remains in some area adherent to the underlying bond coating hence demonstrating the good quality of this ceramic coating. No visible cracks were observed even given the mismatch between in the values of the coefficients of thermal expansion of the particles and the YPSZ matrix. Formation of spinels was observed in the TGO indicating that the Al reservoir of the bond coating is fully depleted. Such phenomenon is attributed to the presence of Al_2O_3 at the intersplat boundaries of the bond coating that formed during plasma spraying process and hinder Al supply from the bond coating to the bond coating/TGO interface [54]. The formation of voluminous Ni/Cr spinels, with high growth rates compared to α-Al_2O_3 [55] is responsible for the local development of stresses leading to the initiation of cracks within the TBC and close to the TGO/TBC interface; see Fig. 7(b).

As can be seen in Fig. 7(b), a crack that initiated at the TGO/TBC interface, propagated through the TBC and interacted with $MoSi_2$ (B) based particles. Image analysis revealed that cracks crossed almost 50% of the particles. This demonstrates a strong adhesion between the protective shell and YPSZ matrix as well as between the protective shell and the core of the particles. Indeed, strong interfaces are needed for the crack to cross the particle instead of propagating at the protective shell/YPSZ interface or being deflected away from the particles [56]. The crack/particle interaction is thus critical for an efficient triggering of the self-healing mechanism.

Fig. 8(a) shows a crack that propagated through the protective shell and the particle, leaving it unprotected against oxidation. At high temperature, i.e. during the hot dwell of the thermal cycle, oxygen diffusing both through the crack pathway and the surrounding YPSZ matrix reacted with the $MoSi_2$ based particle (Eq. (1)). This reaction resulted in the formation of amorphous borosilicate phase (black phase) that flowed into the crack and wetted the YPSZ grains. The driving force for this flow is the high-volume expansion when converting t-$MoSi_2$ (24.3 $cm^3 \cdot mol^{-1}$) [57] into amorphous SiO_2 (28.9 $cm^3 \cdot mol^{-1}$) [58]. The EDS detector did not allow the detection of the presence of B due to its low atomic number, but this element is expected to be present in the silica phase as boron oxide. Finally, the borosilicate phase locally

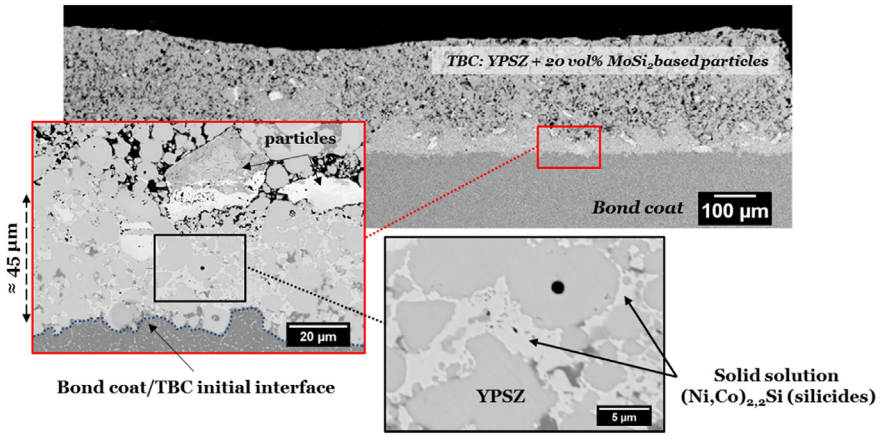

Fig. 5. SEM backscatter electron image of a cross-section of a TBC system as manufactured by spark plasma sintering highlighting the occurrence of a reaction between the $MoSi_2$ based particles and the NiCoCrAlY bond coating leading to the formation of (Ni, Co)$_{2.2}$Si silicide.

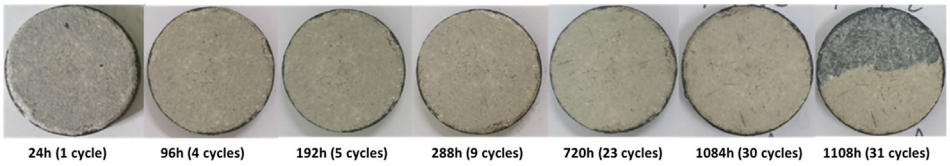

Fig. 6. Evolution of damaging during thermal cycling at 1100 °C of a complete self-healing TBC system made by spark plasma sintering of a mixture of YPSZ powder and 10 vol% encapsulated $MoSi_2$(B) based particles sintered on a NiCrAlY coated substrate.

reacted with the surrounding ZrO_2-based TBC leading to the formation of a new crystalline phase (Eq. (2)), identified by XMA as being zircon. One can clearly observe that $ZrSiO_4$ links the opposite crack surfaces, meaning that the crack is locally healed. The healing mechanism depicted here is in very good agreement with the envisioned self-healing concept and mechanism reported earlier [11]. No molybdenum was detected by XMA in the borosilicate phase meaning that this element escaped the system, most probably as Mo volatile oxides (e.g. MoO_3), through the crack pathway during high temperature exposure. The crack opening distance near the particle is about 0.5–0.6 μm; see Fig. 8(a). Healing of the crack is visible at a distance up to 4.5 μm from the oxidized particle. Complete healing of the crack is not observed due to an insufficient number of crossed particles and thus a limited Si reservoir for silica formation. As mentioned in the experimental part, the TBC is porous (about 20 vol%) and thus a larger amount of silica is necessary to fill the crack and the pores. Fig. 8(b) shows a crack that crossed several particles just above the TBC/TGO interface. The crack length is about 215 μm and the spacing between the particles is about 15 μm and filled with a SiO_2(-B_2O_3) phase. Not all the crack is filled with borosilicate phase and this phase was only partially converted into zircon. However, even if the crack is not fully healed, it might be enough to limit the damage to a non-catastrophic level and prevent further propagation of the crack.

4.4. Stability of the healing particles

Many particles remained intact after long exposure at high temperature as shown in Fig. 7 and Fig. 8(b). Consequently, and despite the fact that the shell is not only pure α-Al_2O_3, the shell offers good protection to the particles core. This observation is important because a good thermal stability of the particles is necessary to ensure healing ability of the TBC even after long exposure at high temperature in an oxidizing environment. A continuous layer of zircon (grey phase) can be observed around the particles; see Fig. 7(b). This zircon layer may be responsible for the oxidation resistance of the particles by acting as a diffusion barrier against oxygen [59]. Indeed, the value for the diffusion coefficient of oxygen in $ZrSiO_4$ is several orders smaller than the diffusion coefficient of oxygen in SiO_2-B_2O_3 [42,45–47].

In this work, it is shown that after sintering and short annealing, the alumina shell deposited around the $MoSi_2$(B) particles is not composed of pure α-Al_2O_3 but is a mixture of different oxides, among them a continuous layer of borosilicate. Since $MoSi_2$ oxidizes spontaneously, even

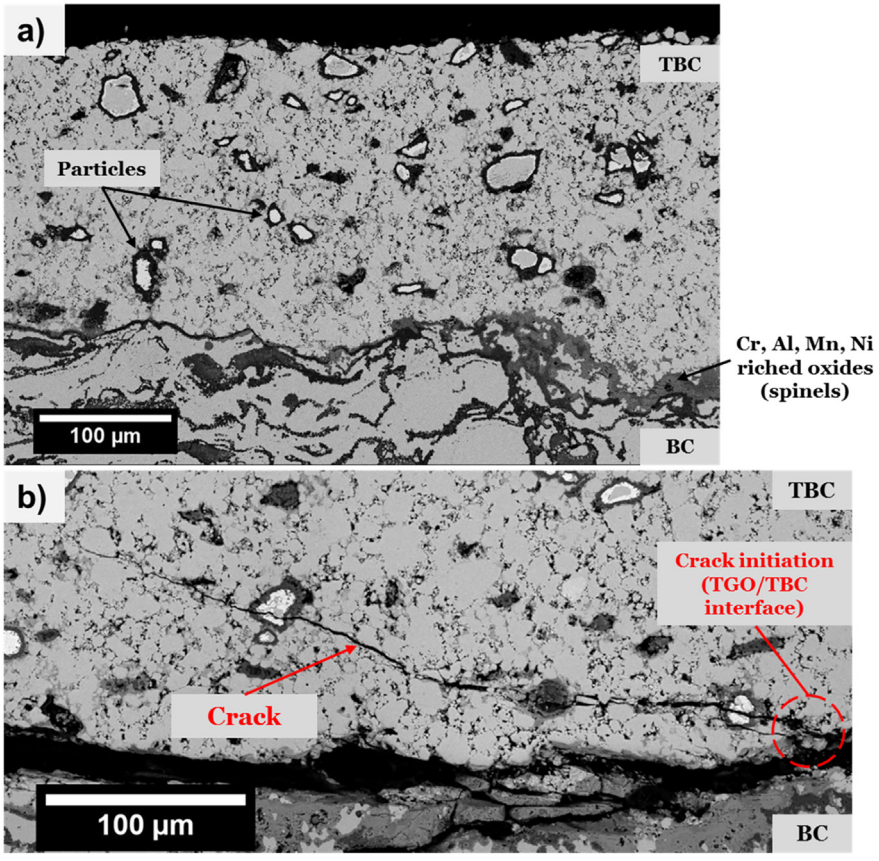

Fig. 7. SEM backscattered images of cross-section views of a TBC made of a mixture of YPSZ powder and 10 vol% encapsulated $MoSi_2$(B) based particles sintered on a NiCrAlY coated substrate after 1108 cumulated hot hours at 1100 °C (31 cycles): (a) uncracked area, (b) cracked area near the spalled area.

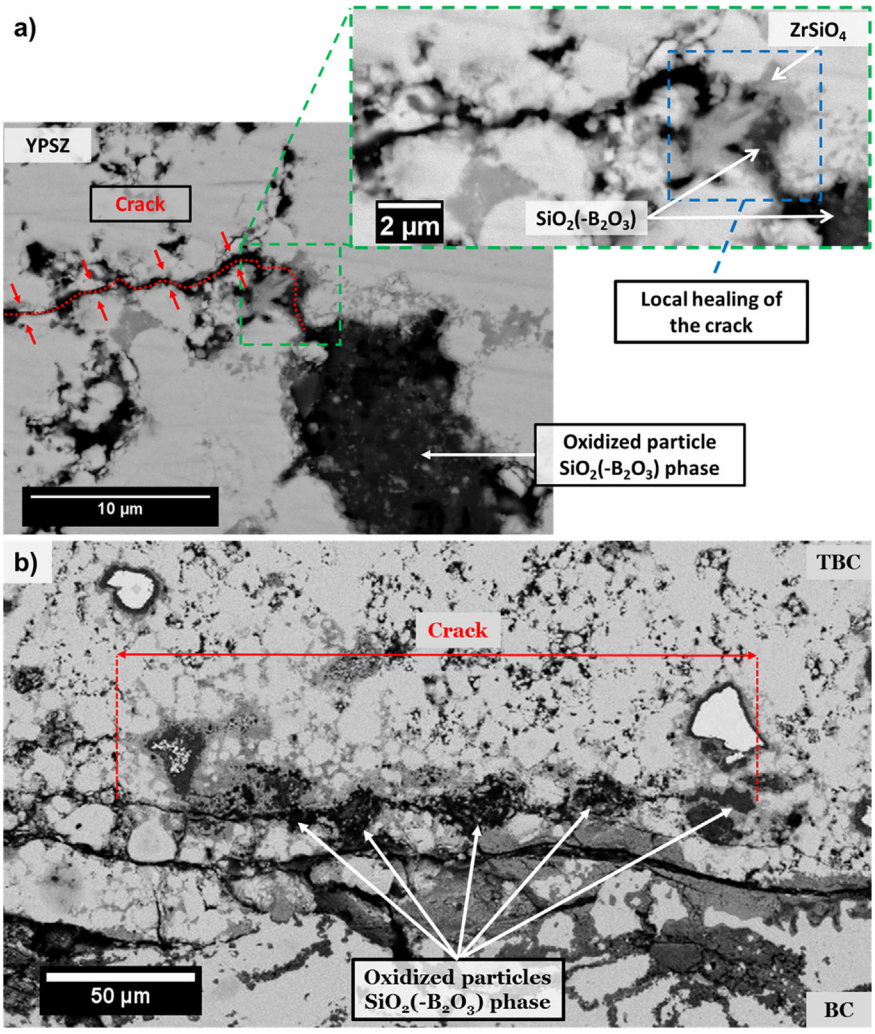

Fig. 8. SEM backscatter electron image of a cross-section view of a TBC made of: (a) a mixture of YPSZ and 5 vol% of encapsulated $MoSi_2$(B) based particles after 151 cycles of 1 h at 1100 °C, and (b) a mixture of YPSZ powder and 10 vol% encapsulated $MoSi_2$(B) based particles sintered on a NiCrAlY coated substrate after 1108 cumulated hot hours at 1100 °C (31 cycles).

in the absence of cracks, the size of the particles is expected to decrease drastically with time. Carter developed a kinetic model for solid-gas or solid-solid reactions between spherical particles and gas or fine-particles [60]. In this model, it is assumed that the oxidation reaction is controlled by diffusion through the oxide layer. The oxidation rate of the spherical particles is given by Eq. (3).

$$t = \frac{r_0^2}{2(z-1)k}\left\{z-(z-1)(1-x)^{\frac{2}{3}}-[1+(z-1)x]^{\frac{2}{3}}\right\} \quad (3)$$

where t is time, r_0 is the initial radius of the particle at the initial stage (i.e., $t = 0$), z is the relative volume expansion when the metal reacts to form the oxide or Pilling-Bedworth ratio, k is the parabolic rate constant and x the oxidation ratio (i.e., the fraction of the particle which has oxidized).

In the present work, it is assumed that the $MoSi_2$ based particles are nearly spherical, with a r_0 value of 8 µm and covered by a uniform borosilicate oxide scale. Furthermore, it is considered that the Si consumed from the particle is used to grow this scale and that all the remaining Mo escapes from the particles presumably as volatile Mo oxides. The formation of a Mo rich phase (i.e., Mo_5Si_3) is neglected. This implies that at each time, the system is composed of a spherical $MoSi_2$ particle covered with a uniform borosilicate scale.

Eq. (3) was solved numerically using a z value of 2.4 (as obtained from the molar volumes of $MoSi_2$ and SiO_2, respectively; cf. [11]) and k value of 5.0×10^{-5} µm^2·s^{-1} corresponding to the parabolic constant for the growth of SiO_2-B_2O_3 on a $MoSi_2$ substrate alloyed with 2 wt% B [23]. The dependence of the oxidation ratio (x) with time (t) is given in Fig. 9. Experimental oxidation ratio (x_{exp}) values satisfy $r^3 = (1 - x_{exp})r_0^3$ where r is the instantaneous radius of the $MoSi_2$ spherical particle. The r values were determined from SEM cross-sections of the TBCs after thermal cycling and using image analysis. One can observe, from data derived from the kinetic model (Eq. (3)), that in the case of a particle covered with a borosilicate oxide scale, the particle is fully consumed ($x = 1$) after 77 h cumulated hours at 1100 °C. Full consumption of unprotected particles after only 77 h dismisses them as healing agents in TBC systems for long duration exposure in an oxidizing environment. Furthermore, almost half of the particle is consumed after 10 h. A k value (Eq. (3)) of 5.3×10^{-7} µm^2·s^{-1} was found to fit best the experimental data. This value is almost 100 times smaller than the one obtained for a uniform layer of SiO_2-B_2O_3 (5.0×10^{-5} µm^2·s^{-1} [23]). This demonstrates the stability of the encapsulated particles and the possibility to use them as healing agents for long exposure times under service conditions.

5. Conclusions

The protocol for manufacturing a new self-healing TBC made of YPSZ and core-shell encapsulated $MoSi_2$(B) based particles by spark plasma sintering as well as its healing behaviour is presented. A self-healing

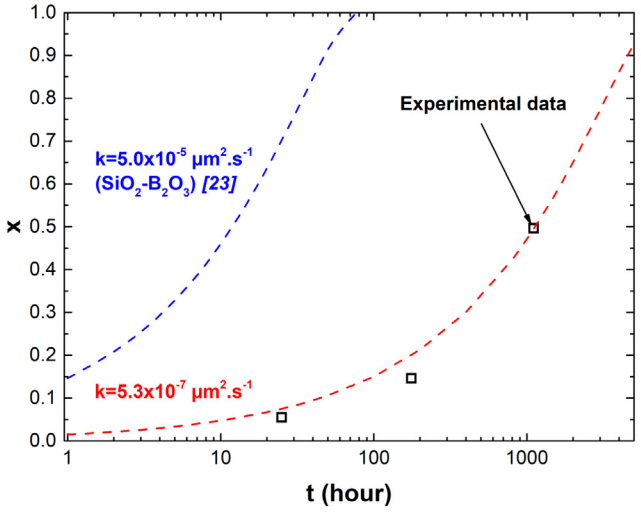

Fig. 9. Evolution of the oxidation ratio (x) of spherical $MoSi_2$ based particles as a function of time at a temperature of 1100 °C.

TBC made of a mixture of YPSZ powder and encapsulated $MoSi_2$ (B) based particles has been applied on MCrAlY coated Ni based superalloys using spark plasma sintering. SEM observations of cross-section of the SPS sintered TBC revealed that no cracks were present resulting from thermally induced stresses due to difference in CTE of $MoSi_2$ based particles and YPSZ matrix.

Pre-oxidation of the MCrAlY coated substrates is necessary to form an α-Al_2O_3 oxide scale that prevents the formation of silicides. It is observed that exposure of $MoSi_2$ based particles in contact with or close enough to the MCrAlY layer at high temperature is responsible for the formation of brittle and fast-growing Ni/Co silicides. Such formation leads to early spallation of the TBC.

After short exposure to high temperature, the α-Al_2O_3 shell that initially covered the particles is converted to a much more complex shell. It consists of an overlap of silica or borosilicate oxides, γ-Al_2O_3 and $ZrSiO_4$ crystallites, and Si enriched ZrO_2 oxide scale. Despite the higher oxygen diffusivity in the aforementioned oxides compared to α-Al_2O_3, this multi-layer and multi-oxide shell offers a good protection against oxidation of the $MoSi_2$(B) based healing particles. When such a protective shell is present, the particles oxidize at a rate almost 100 times slower than unprotected $MoSi_2$(B) based particles.

The self-healing TBC samples exhibit a good resistance against thermal cycling at 1100 °C in air, which demonstrates the feasibility and the good performance of this TBC made by spark plasma sintering. Post-mortem observations in the cracked areas of the TBC showed that some cracks are partially filled with borosilicate or silicate phase and a zircon phase that connects both surfaces of the crack. These observations confirm the intended self-healing mechanism of $MoSi_2$(B) based particles reinforced yttria partially stabilized zirconia based TBCs.

Acknowledgments

This project has received funding from European Union Seventh Framework Program (FP7/2007–2013) under grant agreement no. 309849, SAMBA. The authors thank M.C. Lafont for the TEM work performed at CIRIMAT laboratory, and Ing. R. W. A. Hendrikx for the XRD analysis at Delft University of Technology.

References

[1] R.A. Miller, Thermal barrier coatings for aircraft engines: history and directions, J. Therm. Spray Technol. 6 (1997) 35–42.
[2] J. DeMasi-Marcin, Thermal barrier coating experience in gas turbine Engines at Pratt & Whitney, J. Therm. Spray Technol. 6 (1997) 99–104.
[3] M. Stiger, N. Yanar, M. Topping, F. Pettit, Thermal barrier coatings for the 21st century, Zeitschrift Für Met. 90 (1999) 1069–1078.
[4] N.P. Padture, M. Gell, Thermal barrier coatings for gas-turbine engine applications, Sci. Compass. (2002) 280–284.
[5] A.G. Evans, D.R. Mumm, J.W. Hutchinson, G.H. Meier, F.S. Pettit, Mechanisms controlling the durability of thermal barrier coatings, Prog. Mater. Sci. 46 (2001) 505–553.
[6] F. Yao, K. Ando, M.C. Chu, S. Sato, Static and cyclic fatigue behaviour of crack-healed Si_3N_4/SiC composite ceramics, J. Eur. Ceram. Soc. 21 (2001) 991–997.
[7] K. Takahashi, M. Yokouchi, S.-K. Lee, K. Ando, Crack-healing behavior of Al_2O_3 toughened by SiC whiskers, J. Am. Ceram. Soc. 86 (2003) 2143–2147.
[8] M.C. Chu, S. Sato, Y. Kobayashi, K. Ando, Damage healing and strengthening behaviour in intelligent mullite/SiC ceramics, Fatigue Fract. Eng. Mater. Struct. 18 (1995) 1019–1029.
[9] A.L. Salas-Villasenor, J. Lemus-Ruiz, M. Nanko, D. Maruoka, Crack disappearance by high-temperature oxidation of alumina toughened by Ni nano-particles, Adv. Mater. Res. 68 (2009) 34–43.
[10] Z. Derelioglu, A.L. Carabat, S. Van Der Zwaag, On the use of B-alloyed $MoSi_2$ particles as crack healing agents in yttria stabilized zirconia thermal barrier coatings, J. Eur. Ceram. Soc. 35 (2015) 4507–4511.
[11] V. Kochubey, W.G. Sloof, Self healing mechanism in thermal barrier coatings, Proc. Int. Therm. Spray Conf, 2008.
[12] S.J. Skinner, J.A. Kilner, Oxygen ion conductors, Mater. Today 6 (2003) 30–37.
[13] A.J. McEvoy, Thin SOFC electrolytes and their interfaces: a near-term research strategy, Solid State Ionics 132 (2000) 159–165.
[14] A.L. Carabat, S. van der Zwaag, W.G. Sloof, Creating a protective Shell for reactive $MoSi_2$ particles in high-temperature ceramics, J. Am. Ceram. Soc. 98 (2015) 2609–2616.
[15] A.L. Carabat, M.J. Meijerink, J.C. Brouwer, E.M. Kelder, J.R. van Ommen, S. van der Zwaag, W.G. Sloof, Protecting the $MoSi_2$ Healing Particles for Thermal Barrier Coatings Using a Sol-Gel Produced Al_2O_3 Coating (to be Publ.) 2018.
[16] D. Koch, Atmospheric Plasma Spraying of Self-Healing Thermal Barrier Coatings, Int. Therm. Spray Conf. Expo., 2015
[17] C. Elissalde, M. Maglione, C. Estournès, Tailoring dielectric properties of multilayer composites using spark plasma sintering, J. Am. Ceram. Soc. 90 (2007) 973–976.
[18] D. Monceau, D. Oquab, C. Estournes, M. Boidot, S. Selezneff, Y. Thebault, Y. Cadoret, Pt-modified Ni aluminides, MCrAlY-base multilayer coatings and TBC systems fabricated by Spark Plasma Sintering for the protection of Ni-base superalloys, Surf. Coat. Technol. 204 (2009) 771–778.
[19] J. Song, K. Ma, L. Zhang, J.M. Schoenung, Simultaneous synthesis by spark plasma sintering of a thermal barrier coating system with a NiCrAlY bond coat, Surf. Coat. Technol. 205 (2010) 1241–1244.
[20] F. Nozahic, Elaboration Par Spark Plasma Sintering et caractérisation de Composites et Multi-Couches Zircone yttrié/$MoSi_2$(B) Pour Application barrière Thermique Auto-Cicatrisante, Université de Toulouse - Institut National Polytechnique de Toulouse, 2016http://oatao.univ-toulouse.fr/17475/.
[21] A.H. Pakseresht, A.H. Javadi, M. Bahrami, F. Khodabakhshi, A. Simchi, Spark plasma sintering of a multilayer thermal barrier coating on Inconel 738 superalloy: microstructural development and hot corrosion behavior, Ceram. Int. 42 ((2016) 2770–2779.
[22] F. Nozahic, D. Monceau, C. Estournès, Thermal cycling and reactivity of a $MoSi_2/ZrO_2$ composite designed for self-healing thermal barrier coatings, Mater. Des. 94 (2016) 444–448.
[23] F. Nozahic, A.L. Carabat, W. Mao, C. Kwakernaak, S. van der Zwaag, W.G. Sloof, C. Estournes, D. Monceau, The Effect of Boron on Zircon Formation in Extrinsic Self-Healing Thermal Barrier Coatings(to be Publ.) 2018.
[24] D. Monceau, F. Crabos, A. Malié, B. Pieraggi, Effects of bond-coat preoxidation and surface finish on isothermal and cyclic oxidation, high temperature corrosion and thermal shock resistance of TBC systems, Mater. Sci. Forum 369–372 (2001) 607–614.
[25] M. Boidot, Elaboration de revêtements γ-γ' et de systèmes barrière thermique par Spark Plasma Sintering, Université de Toulouse - Institut National Polytechnique de Toulouse, 2010http://ethesis.inp-toulouse.fr/archive/00001693/01/boidot.pdf.
[26] C. Manière, A. Pavia, L. Durand, G. Chevallier, K. Afanga, C. Estournès, Finite-element modeling of the electro-thermal contacts in the spark plasma sintering process, J. Eur. Ceram. Soc. 36 (2016) 741–748.
[27] K. Vanmeensel, A. Laptev, O. Van der Biest, J. Vleugels, Field assisted sintering of electro-conductive ZrO_2-based composites, J. Eur. Ceram. Soc. 27 (2007) 979–985.
[28] S. Selezneff, Etude et développement de revêtements γ-γ' riches en platine, élaborés par Spark Plasma Sintering (SPS), Application au système barrière thermique, Université de Toulouse - Institut National Polytechnique de Toulouse, 2011http://oatao.univ-toulouse.fr/16567/.
[29] T. Gheno, Oxydation et carburation d'alliages modèles chromino-formeurs dans le dioxyde de carbone, Université de Toulouse - Institut National Polytechnique de Toulouse, 2012http://www.theses.fr/2012INPT0060.
[30] X.Q. Cao, R. Vassen, D. Stoever, Ceramic materials for thermal barrier coatings, J. Eur. Ceram. Soc. 24 (2004) 1–10.
[31] A.K. Vasudévan, J.J. Petrovic, A comparative overview of molybdenum disilicide composites, Mater. Sci. Eng. A 155 (1992) 1–17.
[32] Y.T. Zhu, M. Stan, S.D. Conzone, D.P. Butt, Thermal oxidation kinetics of $MoSi_2$-based powders, J. Am. Ceram. Soc. 82 (1999) 2785–2790, https://doi.org/10.1111/j.1151-2916.1999.tb02156.x.
[33] D.A. Berztiss, R.R. Cerchiara, E.A. Gulbransen, F.S. Pettit, G.H. Meier, Oxidation of $MoSi_2$ and comparison with other silicide materials, Mater. Sci. Eng. A 155 (1992) 165–181.
[34] J. Cook, A. Khan, E. Lee, R. Mahapatra, Oxidation of $MoSi_2$-based composites, Mater. Sci. Eng. A 155 (1992) 183–198.

[35] M.K. Meyer, A. Mufit, Oxidation behavior of boron modified Mo_5Si_3 at 800–1300 °C, J. Am. Ceram. Soc. 79 (1996) 938–944.
[36] M. Meyer, M. Kramer, M. Akinc, Boron-doped molybdenum silicides, Adv. Mater. 8 (1996) 85–88.
[37] M.G. Mendiratta, T.A. Parthasarathy, D.M. Dimiduk, Oxidation behavior of αMo–Mo_3Si–Mo_5SiB_2 (T2) three phase system, Intermetallics 10 (2002) 225–232.
[38] V. Supatarawanich, D. Johnson, C. Liu, Effects of microstructure on the oxidation behavior of multiphase Mo–Si–B alloys, Mater. Sci. Eng. A 344 (2003) 328–339.
[39] T. Itoh, Formation of polycristalline zircon ($ZrSiO_4$) from amorphous silica and amorphous zirconia, Cryst. Growth Des. 125 (1992) 223–228.
[40] W. Mao, W. Sloof, Kinetics of self-healing reaction in TBC with $MoSi_2$ based sacrificial particles, 2013.
[41] X. Li, B. Hafskjold, Molecular dynamics simulations of yttrium-stabilized zirconia, J. Phys. Condens. Matter 7 (1995) 1255.
[42] J. Schlichting, Oxygen transport through glass layers formed by a gel process, J. Non-Cryst. Solids 63 (1984) 173–181.
[43] P. Fielitz, G. Borchardt, H. Schneider, M. Schmücker, M. Wiedenbeck, D. Rhede, Self-diffusion of oxygen in mullite, J. Eur. Ceram. Soc. 21 (2001) 2577–2582.
[44] A.H. Heuer, T. Nakagawa, M.Z. Azar, D.B. Hovis, J.L. Smialek, B. Gleeson, N.D.M. Hine, H. Guhl, H.S. Lee, P. Tangney, W.M.C. Foulkes, M.W. Finnis, On the growth of Al_2O_3 scales, Acta Mater. 61 (2013) 6670–6683.
[45] Y.-F. Zheng, B. Fu, Estimation of oxygen diffusivity from anion porosity in minerals, Geochem. J. 32 (1998) 71–89.
[46] B. Zhang, X. Wu, Prediction of self-diffusion and heterodiffusion coefficients in zircon, J. Asian Earth Sci. 42 (2011) 134–141.
[47] E.B. Watson, D.J. Cherniak, Oxygen diffusion in zircon, Earth Planet. Sci. Lett. 148 (1997) 527–544.
[48] M.A. Lamkin, F.L. Riley, R.J. Fordham, Oxygen mobility in silicon dioxide and silicate glasses: a review, J. Eur. Ceram. Soc. 10 (1992) 347–367.
[49] T.G. Finstad, A Xe marker study of the transformation of Ni_2Si to NiSi in thin films, Phys. Status Solidi 63 (1981) 223–228.
[50] W.K. Chu, S.S. Lau, J.W. Mayer, H. Müller, K.N. Tu, Implanted noble gas atoms as diffusion markers in silicide formation, Thin Solid Films 25 (1975) 393–402.
[51] F. d'Heurle, S. Petersson, L. Stolt, B. Strizker, Diffusion in intermetallic compounds with the CaF_2 structure: a marker study of the formation of $NiSi_2$ thin films, J. Appl. Phys. 53 (1982) 5678–5681.
[52] G.J. van Gurp, W.F. van der Weg, D. Sigurd, Interactions in the Co/Si thin-film system. II. Diffusion-marker experiments, J. Appl. Phys. 49 (1978) 4011–4020.
[53] P. Nash, A. Nash, The Ni-Si (Nickel-Silicon) system, Bull. Alloy Phase Diagr. 8 (1987) 6–14.
[54] H.E. Evans, M.P. Taylor, Diffusion cells and chemical failure of MCrAlY bond coats in thermal-barrier coating systems, Oxid. Met. 55 (2001) 17–34.
[55] D.J. Young, High temperature oxidation and corrosion of metals, in: T. Burnstein (Ed.), Elsevier Corros. Ser. Elsevier, Amsterdam 2008, p. 318.
[56] W.G. Sloof, S.R. Turteltaub, A.L. Carabat, Z. Derelioglu, S.A. Ponnusami, G.M. Song, Crack Healing in Yttria Stabilized Zirconia Thermal Barrier Coatings, Self Heal. Mater. - Pioneer. Res., Netherlands, 2015 217–225.
[57] P. Villars, Pearson's Crystal Data®: Crystal Structure Database for Inorganic Compounds, ASM International, 2007.
[58] D. Krause, Glasses, in: W. Martienssen, H. Warlimont (Eds.), Springer Handb. Condens. Matter Mater. Data, Springer 2005, p. 527.
[59] C. Wang, K. Li, X. Shi, J. Sun, Q. He, C. Huo, Self-healing YSZ-La-Mo-Si heterogeneous coating fabricated by plasma spraying to protect carbon/carbon composites from oxidation, Compos. Part B Eng. 125 (2017) 181–194.
[60] R.E. Carter, Kinetic model for solid-state reactions, J. Chem. Phys. 34 (1961) 2010–2015.